Received Date : 26-Sep-2016
Revised Date : 13-Jan-2017
Accepted Date : 17-Jan-2017
Article type : Original Article

Comparative RNA-Seq Transcriptome Analyses Reveal Distinct Metabolic Pathways in Diabetic Nerve and Kidney Disease

Lucy M. Hinder1[$], Meeyoung Park[1$], Amy E. Rumora[1$], Junguk Hur[5], Felix Eichinger[2], Subramaniam Pennathur[2], Matthias Kretzler[2,3], Frank C. Brosius III[2,4] and Eva L. Feldman[1*]

Departments of [1]Neurology, [2]Internal Medicine, [3]Computational Medicine and Bioinformatics, [4]Molecular and Integrative Physiology, University of Michigan, Ann Arbor, MI 48109, USA
[5]Department of Biomedical Sciences, University of North Dakota, School of Medicine and Health Sciences, Grand Forks, ND 58202, USA
[$]These authors contributed equally.

[*]Corresponding author:
Eva L. Feldman, MD, PhD, Russell N. DeJong Professor of Neurology
5017 AAT-BSRB, 109 Zina Pitcher Place, Ann Arbor, Michigan 48109, United States
Phone: (734) 763-7274 / Fax: (734) 763-7275, Email: efeldman@umich.edu

ABSTRACT

Treating insulin resistance with pioglitazone normalizes renal function and improves small nerve fiber function and architecture; however, it does not affect large myelinated nerve fiber function in mouse models of type 2 diabetes (T2DM), indicating that pioglitazone affects the body in a tissue-specific manner. To identify distinct molecular pathways regulating diabetic peripheral neuropathy (DPN) and nephropathy (DN), as well those affected by pioglitazone, we assessed DPN and DN gene transcript expression in control and diabetic mice with or without pioglitazone treatment. Differential expression analysis and Self-Organizing Maps were then used in parallel to analyze transcriptome data. Differential expression analysis showed that gene expression promoting cell death and the inflammatory response was reversed in the kidney glomeruli but unchanged or exacerbated in sciatic nerve by pioglitazone. Self-Organizing Map analysis revealed that mitochondrial dysfunction was normalized in kidney and nerve by treatment; however, conserved pathways were opposite in their directionality of regulation. Collectively, our data suggest inflammation may drive large fiber dysfunction, while mitochondrial dysfunction may drive small fiber dysfunction in T2DM. Moreover, targeting both of these pathways is likely to improve DN. This study supports growing evidence that systemic metabolic changes in T2DM are associated with distinct tissue-specific metabolic reprogramming in kidney and nerve, and that these changes play a critical role in DN and small fiber DPN pathogenesis. These data also highlight the potential dangers of a “one size fits all” approach to T2DM therapeutics, as the same drug may simultaneously alleviate one complication while exacerbating another.

KEYWORDS

Type 2 Diabetes, Diabetic Peripheral Neuropathy, Diabetic Nephropathy, Pioglitazone

INTRODUCTION

Type 2 diabetes mellitus (T2DM) affects over 387 million people worldwide [1] and its prevalence continues to increase [2]. T2DM itself is a complex metabolic disease characterized by hyperglycemia, hyperlipidemia, and impaired insulin signaling that develops as a result of genetic factors, obesity, or the environment. As T2DM progresses, oxidative stress, high circulating blood glucose levels, and hyperlipidemia can promote microvascular complications that can result in severe debility and

increased mortality. These complications are one of the greatest challenges facing the healthcare industry: in 2014 alone the global medical expenditure for diabetic patients totaled over $245 billion, with 25-45% of those costs related to associated vascular complications [3].

The most common of these microvascular complications include diabetic peripheral neuropathy (DPN) and diabetic nephropathy (DN) [4,5]. DPN affects 50% of diabetic patients and is characterized by progressive loss of sensation in the limbs, pain, and allodynia. DPN progression also increases the risk of infection and foot ulcers that can lead to amputation of the affected limb [6]. There is no cure for DPN and treatments are limited to glycemic control and symptomatic relief [4]. Similarly, DN affects approximately 40% of diabetic patients. Marked by albuminuria and impaired glomerular filtration, DN is the leading cause of end-stage renal disease in the U.S. [7] and is primarily responsible for the increased mortality in T2DM [8]. Thus, there is a critical need for effective therapeutics and a better understanding of the mechanisms underlying T2DM complications.

Pioglitazone is a drug that is often prescribed to treat T2DM [9,10]. In T2DM animal models, pioglitazone ameliorates DN and diabetic retinopathy via multiple pathways [9,11-16] and can attenuate neuropathic pain and nervous system inflammation [17,18]. Mechanistically, pioglitazone acts as an agonist of peroxisome proliferator-activated receptor gamma (PPARG), but it differentially regulates metabolism in a tissue-specific manner [19]. We recently reported that pioglitazone normalized the renal function and significantly improved small nerve fiber function in the C57BLKS-*db/db* murine model of T2DM [20]. However, pioglitazone had no effect on the phenotypical measurement of large myelinated fiber function.

In the current study, we expand on our previous findings by evaluating gene expression changes in both the nerve and kidney from control (*db/+*), diabetic (*db/db)*, and pioglitazone-treated (*db/+* PIO and *db/db* PIO) mice using RNA-Sequencing (RNA-Seq); we subsequently analyze these changes using both differential analysis [20] and Self-Organizing Maps (SOMs) [21-23]. This combination of analyses, tissues, and treatment represents several important advances over previous studies examining diabetes and pioglitazone. First, RNA-Seq provides more complete transcriptomic information than microarray analysis and is much more sensitive and specific [24]. Second, we expand our tissue analysis to include the kidney which provides key information into the mechanisms of DN as well as pioglitazone treatment. Third, the simultaneous analysis and subsequent comparison of both nervous and renal tissue allows us to assess the tissue-specific effects of pioglitazone as well as the basic mechanisms underlying diabetic complications in peripheral tissue. Finally, the parallel use of two forms of RNA-Seq analysis will alleviate the wide variety of results that can be generated using common software packages [25,26].

MATERIALS AND METHODS

Animals

Male C57BLKS (BKS) *db/+* and *db/db* mice (BKS.Cg-m+/+Lepr^{db}/J; stock number 000642) (Jackson Laboratory, Bar Harbor, ME) were fed a standard diet (AIN76A; 11.5% kcal fat; Research Diets, New Brunswick, NJ) and cared for in a pathogen-free environment by the University of Michigan Unit for Laboratory Animal Medicine. Mice were treated with or without 15 mg/kg pioglitazone (112.5 mg pioglitazone/kg chow for a dose of 15 mg/kg to the mouse) between 5 and 16 weeks of age, for 11 total weeks (Figure 1A). Animal protocols were approved by the University of Michigan University Committee on Use and Care of Animals and complied with Diabetic Complications Consortium guidelines (https://www.diacomp.org/shared/protocols.aspx).

Metabolic phenotyping

For each animal, body weight was recorded and fasting blood glucose (FBG) levels were measured with an AlphaTrak Glucometer (Abbott Laboratories, Abbott Park, IL) weekly. Glycated hemoglobin (GHb) levels were determined using a Glyco-Tek Affinity column (catalog no. 5351; Helena Laboratories, Beaumont, TX) at the Michigan Diabetes Research and Training Center Chemistry Core. Fasting plasma insulin, total cholesterol, and total triglycerides were measured by the National Mouse Metabolic Phenotyping Center (Vanderbilt University, Nashville, TN).

DPN and DN phenotyping

All animals were phenotyped for DPN and DN according to Diabetic Complications Consortium guidelines [27,28]. Motor (sciatic) and sensory (sural) nerve conduction velocities (NCVs) were measured for large nerve fiber function, and hind paw withdrawal latency from a thermal stimulus was measured for small fiber function using our published protocols [29,30]. The periodic acid-Schiff (PAS) staining on 3 µm-thick fixed kidney slices determined mesangial area as previously described [31,32]. Urinary albumin levels, albumin/creatinine ratios, glomerular area, and glomerular PAS-positive area were measured using our published protocols [33,34].

RNA-Seq

To identify mechanisms affected by pioglitazone in DPN and DN at the transcriptomic level, we analyzed steady state gene expression using RNA-Seq (Figure 1B). Total RNA was isolated from sciatic nerve (SCN), dorsal root ganglia (DRG), and kidney glomeruli (Glom) and cortex from *db/+* (*n* = 6), *db/db* (*n* = 6), *db/+* PIO (*n* = 6), and *db/db* PIO (*n* = 6) mice. RNA quality was assessed using TapeStation (Agilent, Santa Clara, CA). Samples with RNA Integrity Numbers ≥8 were prepared using the Illumina TruSeq mRNA Sample Prep v2 kit (Catalog #s RS-122-2001, RS-122-2002; Illumina, San Diego, CA). Multiplex amplification was used to prepare cDNA with a paired-end read length of 100 bases using an Illumina HiSeq 2000 (Illumina, Inc., San Diego, CA). RNA sequencing was performed by the University of Michigan DNA Sequencing Core (http://seqcore.brcf.med.umich.edu/).

Quality control assessment of RNA-Seq data was completed using the FastQC tool (http://www.bioinformatics.babraham.ac.uk/projects/fastqc/) for high throughput sequencing before and after RNA-Seq alignment. Then, RNA-Seq data were analyzed using the Tuxedo suite of sequence analysis programs, including Bowtie, TopHat, and Cufflinks [35]. Using TopHat, the resulting FASTQ files were aligned to the NCBI reference mouse transcriptome (NCBI 37) to identify known transcripts. Mapped reads were processed using the Cufflinks algorithm to calculate Fragments Per Kilobase of exon per Million mapped reads (FPKM), which accurately reflects the RNA transcript number normalized for RNA length and total number of mapped reads [35].

Differential expression analysis

The output of Cufflinks was loaded into Cuffdiff [35] to quantify differences in expression of combined transcripts for each gene between the groups within each tissue (*db/+* vs. *db/db*, *db/+* vs. *db/+* PIO, *db/+* PIO vs. *db/db* PIO, and *db/db* vs. *db/db* PIO). The differentially expressed genes (DEGs) with a false discovery rate (FDR) cutoff of <0.05 were identified between groups and sets were compared within and across tissues to identify gene expression changes. Analyses focused on *db/+* vs. *db/db* and *db/db* vs. *db/db* PIO DEG sets to identify gene expression changes in *db/db* mice that were reversed, exacerbated, or unaffected by pioglitazone treatment.

SOM analysis

SOM analysis was performed to identify gene clusters with similar expression patterns in kidney and

nerve of *db/+*, *db/db,* and *db/db* PIO mice. SOMs generate a two-dimensional grid and cluster similar patterns of data points into units called modules. FPKM were pre-processed by removing genes with expression values less than $\log_2 3$ and were centered at zero for each gene [36]. Pre-processed FPKM were applied to a SOM using the algorithm implemented in the MATLAB software Neural Networking toolbox [37]. Gene sets having a similar expression pattern were grouped into modules. Each module in the SOM panel was subjected to functional enrichment analysis. Adjacent modules were further combined into clusters that share enriched functions of interest and similar gene expression patterns.

Function and pathway enrichment analysis

Over-represented biological functions from the DEG sets and SOM modules were identified by functional enrichment analysis using the Database for Annotation, Visualization and Integrated Discovery (DAVID 6.7) (http://david.abcc.ncifcrf.gov). Gene Ontology terms and Kyoto Encyclopedia of Genes and Genomes pathways were adopted as the functional terms [38]. A Benjamini-Hochberg corrected P-value <0.05 was used to identify significantly over-represented biological functions in the DEG sets. To visualize results, heat-maps were generated using the most over-represented biological functions for DEG sets of interest. Hierarchical clustering based on significance values was used to represent overall similarity and differences between the DEG sets [39]. Moreover, clusters from SOM analysis were investigated to identify canonical pathways using Ingenuity Pathway Analysis software (IPA, www.qiagen.com/ingenuity). A Benjamini-Hochberg adjusted p-value was calculated using the Fisher's exact test and <0.05 used to identify significantly over-represented canonical pathways.

RNA-Seq qPCR validation

Technical validation of RNA-Seq data was performed on glomerular tissue by quantitative real-time polymerase chain reaction (RT-qPCR) (n=6/group). Biological confirmation was performed on glomerular and SCN tissue (n=6/group). We focused on the SOM cluster, containing genes regulated by diabetes, but reversed by pioglitazone treatment in both kidney glomeruli and SCN (Figure 4, Table 1) as this cluster likely represents pathways that may drive both DN and small nerve fiber dysfunction, and provides insight into conserved pathways in the diabetic kidney and nerve. Our selection of specific genes for RT-qPCR was based on a combination of expression level (FPKM), fold-change, FDR significance, p-values (Supplementary data file). Based on our understanding of mitochondrial substrate metabolism in complications-prone tissue [40-42], and the established role of oxidative stress in diabetic complications [43], we chose two targets encoding components of fatty acid β-oxidation

(*Acaa2*, and *Echs1* encoding the second and last enzymes of β-oxidation) for technical validation, and two targets encoding subunits of complex II, and IV of the mitochondrial electron transport system (*Sdhb*, complex II; *Cox4i1*, complex IV), and a target encoding a mitochondrial peroxynitrite antioxidant enzyme, peroxiredoxin-5 (*Prdx5*) for biological confirmation.cDNA was generated from 40 ng of total RNA (iScript cDNA Synthesis Kit; Bio-Rad, Hercules, CA). RT-qPCR was performed in triplicate using sequence-specific primers (Supplementary Table 16), Power SYBR® Green PCR Master Mix (Applied Biosystems/Life Technologies), and the StepOnePlus™ Real-Time PCR System (Applied Biosystems/Life Technologies). Expression of each gene was calculated from a cDNA titration within each plate (standard curve method), and normalized to the geometric mean of tyrosine 3-monooxygenase/tryptophan 5-monooxygenase activation protein (*Ywhaz*) endogenous reference gene expression. Samples were assayed in triplicate.

Statistical analyses of phenotypic data

Statistical analyses of phenotypic and RT-qPCR data utilized GraphPad Prism Software, Version 6 (GraphPad Software, La Jolla, California). Data were assumed to follow a Gaussian distribution based on the rules for transformation and non-normative data [44]. One-way ANOVA with Tukey's post-test for multiple comparisons or Kruskal-Wallis test with Dunn's post-test for multiple comparisons were used, as appropriate [45]. The correlation matrix was generated from Pearson correlations. Data were considered significant when $p<0.05$. Reported values represent the mean ± SEM.

RESULTS

Bioinformatic workflow and confirmation of pioglitazone efficacy in the kidney and small nerve fibers

To determine the differential effects of pioglitazone on DPN and DN and to elucidate potential mechanisms explaining tissue-specific differences, we compared the metabolic, neurologic, and renal phenotypes of *db/+* and *db/db* mice with and without pioglitazone treatment (Figure 1A). We next identified differentially regulated cellular pathways using differential analysis and SOMs to analyze RNA transcripts from the SCN, DRG, kidney glomeruli, and kidney cortex (Figure 1B). Consistent with our previous studies [20], *db/db* mice receiving pioglitazone treatment were significantly heavier than both *db/+* and *db/db* mice, but had significantly reduced blood glucose levels and GHb % with no

significant effect on insulin, cholesterol, or triglyceride levels (Supplementary Figure 1). Also consistent with our previous study, we found that pioglitazone could significantly prevent small nerve fiber dysfunction, but large nerve fiber dysfunction was unaffected by treatment (Supplementary Figure 2). In contrast, pioglitazone had a significant effect on DN anatomic and physiologic markers of renal function (Supplementary Figures 3 and 4). Due to the positive effect of pioglitazone treatment on hyperglycemia, small fiber dysfunction (hind paw thermal latency), and DN, we performed correlation analyses between these parameters (Supplementary Figure 5; Supplementary data file). All correlations were significant, suggesting a close relationship between glycemia, small fiber dysfunction, and DN. Taken together, these data indicate that pioglitazone treatment selectively affects different aspects of metabolism and functions in a tissue-specific manner during T2DM.

Differential expression analysis of tissue-specific RNA transcripts identifies reversed and exacerbated genes associated with DPN, DN, and pioglitazone treatment

To identify specific mechanisms differentially affected by pioglitazone in DPN and DN at the transcriptomic level, we first analyzed steady-state gene expression in the SCN, DRG, kidney glomeruli, and kidney cortex using RNA-Seq. This analysis resulted in an average of 29.8 (±8.4) million reads, and the resulting data were subsequently analyzed using differential expression analysis (Figure 1B, Supplementary Table 1). For each type of tissue, four DEG sets were obtained from the pairwise comparisons (*db/+* vs. *db/db*, *db/+* vs. *db/+* PIO, *db/+* PIO vs. *db/db* PIO, and *db/db* vs. *db/db* PIO) (Figure 2A). The number of genes regulated by diabetes (*db/+* vs. *db/db)* was similar in the SCN (2,077) and the DRG (2,061); however, pioglitazone significantly changed gene expression in fourteen-fold more genes in the diabetic SCN (2,368) than in the DRG (164). Similarly, in the kidney the number of DEGs was greater in diabetic glomeruli (1,644) than in cortex (909), and pioglitazone changed the expression of four-fold more genes in the diabetic glomeruli (2,880) than the cortex (678). These data indicate that even within similar tissue, pioglitazone treatment can have differing effects.

To better understand the cellular mechanisms driving DN and DPN changes in response to pioglitazone treatment, we next compared *db/+* vs. *db/db* and *db/db* vs. *db/db* pioglitazone DEG sets in each tissue (Figure 2B). Overall, 897 (43%) SCN DEGs and 1,119 (68%) glomeruli DEGs were significantly affected by both diabetes and pioglitazone in *db/db* mice (Supplementary Tables 2-9). However, only 109 (5%) DRG and 155 (17%) kidney cortex DEGs were affected by treatment. To address the discrepancy, we examined the transcript expression of *Ppara*, *Ppard*, and *Pparg* in the SCN, DRG, kidney glomeruli, and kidney cortex (Supplementary Figure 6). Pioglitazone is a PPARG agonist;

therefore, we hypothesized that the low number of genes regulated by pioglitazone treatment in DRG and cortex could be due to low PPAR expression in these tissue types. Overall, the number of *Ppar* transcripts was highest in kidney glomeruli and SCN with reduced expression in the kidney cortex and negligible transcript expression in the DRG. Hence, the reduced *Ppar* expression in the DRG and the kidney cortex likely explain the relatively low numbers of shared DEGs in these tissues. Our subsequent analyses therefore focused primarily on the SCN and glomeruli, as these tissues are affected by pioglitazone treatment.

We next determined whether DEGs shared between the *db/+* vs. *db/db*, and *db/db* vs. *db/db* PIO DEG sets were regulated in the opposite (reversed) or same (exacerbated) direction (Figure 2C). As large fiber dysfunction is unaffected by pioglitazone treatment in *db/db* mice (Supplementary Figure 2), we reasoned that DEGs in SCN that are significantly up-regulated during diabetes but not reversed by pioglitazone treatment (Supplementary Table 2) may contribute to large fiber dysfunction. In contrast, genes reversed by pioglitazone treatment in the SCN (Supplementary Table 7) and reversed in the glomeruli (Supplementary Table 8) may prevent damage of the small nerve fibers and the kidney during T2DM. Consistent with our phenotypic data, only half of the shared DEGs in SCN (49%) were reversed by pioglitazone treatment while the majority of the shared DEGs in glomeruli (95%) were reversed. These data suggest that pioglitazone may contribute to large nerve fiber dysfunction by exacerbating a tissue-specific specific subset of genes within the SCN while ameliorating DN via a completely different mechanism.

Comparison of pathways using differential expression analysis identifies cellular pathways associated with tissue-specific pioglitazone function

We next used the DEGs found in the SCN and kidney glomeruli to determine which cellular pathways are associated with DPN, DN, and pioglitazone treatment. DN phenotypes were completely prevented by pioglitazone (Supplementary Figure 3), while the effects of pioglitazone on DPN were limited to small fiber function (Supplementary Figures 1 and 2). Therefore, to identify unique pathways underlying these tissue-specific differences, we compared the three DEG subsets from SCN that were either (A) not affected by pioglitazone in diabetic mice (SCN *db/db* only), (B) exacerbated by pioglitazone (SCN Exacerbated), or (C) reversed by pioglitazone (SCN Reversed), to DEGs reversed by pioglitazone in the kidney glomeruli (Glom Reversed) (Figure 3A-C). This was done in order to identify pathways associated with large fiber dysfunction, small fiber dysfunction, , and DN. DEGs shared between the SCN *db/db* only and the Glom Reversed sets are genes that may drive large fiber

dysfunction (Figure 3A); there were a total of 117 DEGs shared between these two data sets. DEGs shared between the SCN Exacerbated and the Glom Reversed data sets indicate genes that may drive both DPN and DN but are not reversed in the SCN by pioglitazone (Figure 3B); there were 71 shared DEGs in the data sets. Finally, shared DEGs between the SCN Reversed and the Glom Reversed data sets indicate genes that are reversed in both tissues by pioglitazone. Since small fiber dysfunction is prevented by pioglitazone, overlapping DEGs in this data set may therefore contribute to small fiber dysfunction (Figure 3C). The SCN Reversed and Glom Reversed data set was comprised of 62 DEGs; the top 20 up- and down-regulated shared DEGs for each of the three comparisons are listed in Supplementary Tables 10-15.

In both the SCN *db/db* only vs. Glom Reversed (Figure 3A) and SCN Reversed vs. Glom Reversed (Figure 3C) DEG comparisons, our functional analysis using DAVID identified enriched pathways related to extracellular matrix (ECM) remodeling and focal adhesion (Figure 3D). In the SCN *db/db* only vs. Glom Reversed data sets, we found gene expression changes in collagen, type I, alpha 1 (*Col1a1*), SRC kinase signaling inhibitor 1 (*Srcin1*), and *Spon2*, suggesting that these DEGs may be involved in DN and large fiber dysfunction in DPN (Supplementary Table 11). In contrast, pioglitazone reversed expression of several DEGs in both the SCN and the kidney glomeruli (SCN Reversed vs. Glom Reversed). Bone morphogenetic protein 3 (*Bmp3*), laminin, gamma 2 (*Lamc2*), type VI, alpha 1 collagen (*Col6a1*), and type III, alpha 1 collagen (*Col3a1*) were reversed in both tissue types suggesting that the associated pathways may be involved in DN and DPN small fiber dysfunction (Supplementary Table 15). Together, these data suggest that correcting changes related to tissue remodeling in the glomeruli has a large impact on DN, but the associated pathways have a more complex relationship with regards to the SCN and DPN.

Of particular interest were the differential effects of pioglitazone in nerve and kidney seen in the SCN *db/db* only vs. Glom Reversed (Figure 3A) and SCN Exacerbated vs. Glom Reversed comparisons (Figure 3B; Supplementary Tables 10-13), as these pathways may contribute to the pathogenesis of both DPN and DN (pioglitazone treatment had no effect on large fiber DPN but reversed DN). Among the shared DEGs, there was functional enrichment of multiple categories related to cell death and the inflammatory response (Figure 3D).

Identification of dysregulated molecular pathways associated with pioglitazone treatment in the SCN and glomeruli using Self-Organizing Map analysis

Previous studies have shown that the use of differential expression analysis for analyzing RNA

transcripts can produce very different results depending on a number of factors [25]. To support the results generated using differential expression analysis, we utilized SOM analysis to identify similar patterns of gene expression across the three experimental groups (*db/+*, *db/db*, and *db/db* PIO) in both the SCN and the kidney glomeruli. After removal of very low expression values, 15,588 genes remained for SOM analysis. Genes with similar expression patterns were grouped into modules and plotted as a 7x7 map in order to empirically identify biologically meaningful pathways (Figure 4A). Genes with the most variation across the experimental groups are gathered in the modules in the top left and bottom right corners of the grid map, whereas genes with less variation across groups are gathered around the center of the map. As a screen to identify modules of interest, we performed DAVID for all 49 modules and determined the most over-represented biological functions (Supplementary Figure 7). By combining adjacent modules with similar expression patterns, we were able to define functional clusters of interest and identify pathways associated with diabetic complications and pioglitazone treatment (Figure 4B) (Table 1).

The regulation pattern of genes in modules 42 and 49 is analogous to the differential expression analysis of genes in the SCN Reversed and Glom Reversed groups, and represents conserved pathways that may drive both DN and small nerve fiber dysfunction (Figure 3C). This cluster contained pathways related to mitochondrial dysfunction, oxidative phosphorylation, glycolysis, fatty acid β-oxidation, and the TCA cycle (Table 1). Genes of interest that were reversed included those encoding subunits of the mitochondrial complexes (complex I NADH oxidoreductase, *Ndufa4/12, Ndufb3/4/6//9/10, Ndufv1/3*; complex II, *Sdha, Sdhb*; complex IV, *Cox4i1, Cox5a, Cox6a1, Cox6b1, Cox6c, Cox7a2, Cox7b*; and complex V, *Atp5g3, Atp5b, Atpaf2*), and β-oxidation enzymes (*Acaa2, Echs1*). Notably, although these pathways are conserved across the tissues, they are largely opposite in their directionality of regulation (Figure 4B). Selected genes in the cluster were validated in SCN and glomeruli using RT-qPCR, which demonstrated comparable profiles to the RNA-Seq data (Supplementary Table 16). Collectively, these observations highlight tissue-specific pathways associated not only with diabetes pathogenesis but with pioglitazone treatment.

DISCUSSION

Available treatments for DPN and DN can have variable efficacy in small nerve fibers, large nerve fibers, and kidneys, suggesting that tissue-specific mechanisms occur in response to treatment. We recently reported that pioglitazone, a triglyceride-lowering, insulin-sensitizing PPARG agonist, has differing effects on DPN and DN phenotypes in a mouse model of diabetes [20]. The goal of this study

was therefore to elucidate the shared and unique mechanisms underlying DN and DPN in response to pioglitazone treatment. Using the same experimental paradigm as our previous study, we confirmed our previous observations that pioglitazone prevents small nerve fiber and renal dysfunction but is unable to prevent large nerve fiber dysfunction during DPN. We then used RNA-Seq combined with a combination of differential expression analysis and SOM analysis to determine molecular pathways that may be driving tissue-specific differences.

We evaluated gene expression changes in the nerve and kidney of control (*db/+*), diabetic (*db/db),* and pioglitazone-treated (*db/+* PIO and *db/db* PIO) mice. Differential expression analysis showed that pioglitazone had a greater effect on SCN and kidney glomeruli gene expression than on DRG and cortex profiles, likely due to reduced PPAR expression in the DRG and the kidney cortex. Subsequent analysis therefore focused on SCN and kidney glomeruli. Consistent with the phenotypic data, in the SCN, 897 shared genes were regulated by both diabetes and pioglitazone, with approximately half of the overlapping genes exacerbated and half reversed by pioglitazone. Those reversed by pioglitazone likely contribute to the prevention of small fiber dysfunction, while those exacerbated or unaffected by pioglitazone likely contribute to large fiber dysfunction. In contrast, of the 1,119 shared genes altered in the kidney glomeruli during diabetes, virtually all (95%) were reversed by pioglitazone treatment.

As small fiber dysfunction and DN correlated strongly with glycemia (Supplementary Figure 5), gene expression reversal may be a downstream effect of preventing hyperglycemia (Supplementary Figure 1). It is unclear to what extent the changes seen following pioglitazone treatment are due to direct PPAR inhibition or prevention of hyperglycemia. Therefore, while it is clear that exacerbated changes in the large nerve fiber are directly due to pioglitazone treatment, the prevention of DN and small nerve fiber dysfunction may be partially due to prevention of hyperglycemia. The enhanced expression of *Ppar* isoforms in tissue with high numbers of DEGs (Supplementary Figure 6), however, suggests that *Ppar* inhibition plays a key role in the observed changes. Further studies will be needed to determine the direct impact of systemic metabolic changes on gene expression in the nerve and kidney.

Consistent with previous reports, genes associated with tissue remodeling such as *Grem1*, *Grem2*, and *Spon2* were significantly up-regulated in the kidney glomeruli during diabetes but reversed by pioglitazone (Supplementary Table 8) [46,47]. Similarly, levels of *SPON2*, an ECM protein involved in innate immunity, correlates with DN severity in T2DM patients [48]; we observed increased *Spon2* levels in the diabetic kidney that were reversed by pioglitazone treatment. Our data therefore suggest that changes in tissue remodeling and ECM function within kidney glomeruli are involved in DN pathophysiology but ameliorated by pioglitazone. Many of these pathways are unaffected or even up-regulated in the presence of pioglitazone in the SCN, however. For example, *Col1a1*, *Srcin1*, and

Spon2 are reversed in glomeruli, but are unaffected by pioglitazone in SCN, suggesting a role for these genes in large fiber dysfunction (Supplementary Table 11).

In contrast, expression of other genes associated with tissue remodeling such as *Bmp3*, *Lamc2*, *Col6a1*, and *Col3a1* was reversed in both the kidney glomeruli and the SCN in response to pioglitazone (Supplementary Table 15). This suggests a role for these genes in small fiber dysfunction. Indeed, injection of *Bmp2*-overexpressing fibroblasts can promote sensory nerve remodeling and neurogenic inflammation in C57BL/6 mice [49]. Regardless of large/small fiber stratification, these data implicate dysfunctional ECM signaling and tissue remodeling as shared pathogenic mechanisms between DN and DPN.

Inflammatory pathways are also differentially regulated in DPN and DN. *Mmp12*, part of the inflammatory matrix metalloproteinase family, was up-regulated in the SCN 143-fold during diabetes but unaffected by pioglitazone treatment (Supplementary Table 2), supporting our previous study which demonstrated *Mmp12* up-regulation in the SCN of leptin-deficient BTBR *ob/ob* mice [39]. In contrast, *Mmp12* deletion in diabetic mice reduces kidney glomeruli matrix accumulation and markers of inflammation, suggesting an important but reversible role for MMP12 in driving kidney complications [50].

To confirm these results, we also used SOM analysis to detect tissue-specific transcription changes in the SCN and kidney glomeruli following pioglitazone treatment. We focused on modules 42 and 49 as their shared pattern of gene expression compares genes that are reversed by pioglitazone treatment in both the kidney glomeruli and SCN (analogous to the Glom Reversed and SCN Reversed differential expression analysis in Figure 3C). This pattern offers mechanistic insight into conserved pathways that may drive both DN and small nerve fiber dysfunction in T2DM. Moreover, this gene cluster likely has greater translational relevance as DPN is predominantly a small fiber disease [6].

This SOM cluster showed enriched transcripts related to mitochondrial dysfunction, fatty acid β-oxidation, the TCA cycle, and oxidative phosphorylation (Table 1). These data support our previous transcriptomics finding that SCN energy homeostasis is important in small fiber neuropathy [20]. Indeed, regulation of these transcripts during diabetic complications is consistent with previous reports demonstrating an up-regulation of endothelial mitochondrial metabolism in response to excess substrate [51]. However, the opposite directionality of change (down-regulation and reversal in SCN, up-regulation and reversal in Glom) suggests a more complex relationship with regards to substrate metabolism in diabetic complications-prone tissues. We recognize that additional mechanistic work is required to explore the biological relevance of transcriptomics data; however, this observation parallels our recent report of tissue-specific changes in fatty acid flux and mitochondrial metabolism, *in vivo*, in

nerve and kidney in BKS-*db/db* mice [40]. Whether these changes in transcriptomics and fluxomics are the cause or the result of diabetes is unknown. Indeed, cross-complications metabolic reprogramming is the subject of ongoing work by our group.

Lastly, to investigate the reproducibility of our transcriptomic studies, we identified common DEG sets shared between the current RNA-Seq analysis and our previous microarray DEG study in the SCN and the DRG [20] (Supplementary Figure 8A). The number of overlapping DEGs between the studies was relatively low during diabetes (*db/+* vs. *db/db*: 411 SCN and 241 DRG) and following pioglitazone treatment (*db/db* vs. *db/db* PIO: 1,408 SCN and 392 DRG). This may reflect differences in the animal models, the platforms, or both. Also, while our data suggest that RNA-Seq is more sensitive than microarray when detecting DEGs (Supplementary Figure 8B), the enriched pathways detected using both techniques were highly similar despite the relatively low number of overlapping DEGs (Supplementary Figure 8C).

In summary, the current differential expression and SOM analyses suggest that shared pathogenic mechanisms exist between DPN and DN, including ECM dysfunction, tissue remodeling, inflammation, and dysfunctional mitochondrial metabolism. Our data suggest that large fiber dysfunction may be related to inflammation, while mitochondrial metabolism may play a greater role in small fiber pathophysiology in T2DM. Moreover, targeting both of these pathways is likely to improve DN phenotypes. We previously reported that lipid-targeted, insulin-sensitizing pioglitazone therapy improved DN, and small fiber measures of DPN. The current study extends those data to suggest that systemic changes in metabolism in T2DM are also associated with distinct tissue-specific metabolic reprogramming in kidney and nerves (similar pathways regulated, different directionality of regulation), and that these changes play a critical role in DN and small fiber DPN pathogenesis. This new insight highlights the potential dangers of a “one size fits all” approach to T2DM therapeutics, as the same drug may simultaneously alleviate one complication while exacerbating another.

Our analyses therefore have the potential to enhance future treatment of diabetic complications by identifying specific molecular pathways associated with each type of complication.

ACKNOWLEDGEMENTS

We would like to thank Ms. Carey Backus and Mr. John M. Hayes for their expertise in conducting DPN. We would like to thank Dr. Hongyu Zhang and Jharna Saha and for their role in assessing DN in animal models of disease. We thank Ms. Carey Backus, Ms. Faye Mendelson, and Ms. Crystal Pacut for their role in performing RT-qPCR. We also thank Dr. Stacey Sakowski Jacoby and Dr. Benjamin

Murdock for their expert editorial advice. All personnel are located at the University of Michigan. Mouse %GHb measurements were performed at the Chemistry Core of the Michigan Diabetes Research and Training Center at U-M (P30DK020572). Plasma insulin and lipid measurements were performed at The Vanderbilt MMPC (U24 DK059637). Funding was provided by the National Institutes of Health (1DP3DK094292, 1R24082841 to E.L.F., F.C.B., S.P., and M.K.; T32 1T32DK101357-01 to A.E.R.), the Juvenile Diabetes Research Foundation (Post-doctoral Fellowship to L.M.H. and J.H.), the American Diabetes Association (E.L.F.), Novo Nordisk (NNF14SA0006 to E.L.F), the Program for Neurology Research & Discovery (M.P.), George O'Brien Kidney Translational Core Center (P30 DK081943 to F.C.B, M.K and S.P) and the A. Alfred Taubman Medical Research Institute (E.L.F., F.C.B).

L.M.H. directed the study, researched data, contributed to discussion, and wrote the manuscript. M.P. researched data and wrote the manuscript. A.R. contributed to discussion and wrote the manuscript. J.H. researched data and revised the manuscript. F.E. researched data. M.K. and F.C.B. designed and directed the study, contributed to discussion, and wrote the manuscript. S.P contributed to the discussion and wrote the manuscript. E.L.F. designed and directed the study, contributed to discussion, and wrote the manuscript.

E.L.F. is the guarantor of this work and, as such, had full access to all the data in the study and takes responsibility for the integrity of the data and the accuracy of the data analysis.

CONFLICT OF INTEREST

The authors have no conflicts of interest to declare for this work.

REFERENCES

1. International Diabetes Foundation Diabetes atlas, sixth edition. 2014.
2. **Deshpande AD, Harris-Hayes M, Schootman M.** Epidemiology of diabetes and diabetes-related complications. *Physical therapy*. 2008; 88: 1254-64.
3. Centers for Disease Control and Prevention. National Diabetes Statistics Report: Estimates of Diabetes and Its Burden in the United States. *Atlanta, GA: US Department of Health and Human Services*. 2014.
4. **Edwards JL, Vincent AM, Cheng HT, Feldman EL.** Diabetic neuropathy: mechanisms to

management. *Pharmacology & therapeutics*. 2008; 120: 1-34.

5. **Kim B, McLean LL, Philip SS, Feldman EL.** Hyperinsulinemia induces insulin resistance in dorsal root ganglion neurons. *Endocrinology*. 2011; 152: 3638-47.

6. **Callaghan BC, Price RS, Feldman EL.** Distal Symmetric Polyneuropathy: A Review. *JAMA*. 2015; 314: 2172-81.

7. **Saran R, Li Y, Robinson B, Ayanian J, Balkrishnan R, Bragg-Gresham J, Chen J, Cope E, Gipson D, He K.** US Renal Data System 2014 Annual Data Report: Epidemiology of Kidney Disease in the United States. *American journal of kidney diseases: the official journal of the National Kidney Foundation*. 2015; 65: A7.

8. **Afkarian M, Sachs MC, Kestenbaum B, Hirsch IB, Tuttle KR, Himmelfarb J, de Boer IH.** Kidney disease and increased mortality risk in type 2 diabetes. *Journal of the American Society of Nephrology*. 2013: ASN. 2012070718.

9. **Goldberg RB, Kendall DM, Deeg MA, Buse JB, Zagar AJ, Pinaire JA, Tan MH, Khan MA, Perez AT, Jacober SJ.** A comparison of lipid and glycemic effects of pioglitazone and rosiglitazone in patients with type 2 diabetes and dyslipidemia. *Diabetes care*. 2005; 28: 1547-54.

10. **Betteridge DJ.** Effects of pioglitazone on lipid and lipoprotein metabolism. *Diabetes, Obesity and Metabolism*. 2007; 9: 640-7.

11. **Nakamura T, Ushiyama C, Osada S, Hara M, Shimada N, Koide H.** Pioglitazone reduces urinary podocyte excretion in type 2 diabetes patients with microalbuminuria. *Metabolism*. 2001; 50: 1193-6.

12. **Schneider CA, Ferrannini E, DeFronzo R, Schernthaner G, Yates J, Erdmann E.** Effect of pioglitazone on cardiovascular outcome in diabetes and chronic kidney disease. *Journal of the American Society of Nephrology*. 2008; 19: 182-7.

13. **Nakamura T, Ushiyama C, Shimada N, Hayashi K, Ebihara I, Koide H.** Comparative effects of pioglitazone, glibenclamide, and voglibose on urinary endothelin-1 and albumin excretion in diabetes patients. *Journal of diabetes and its complications*. 2000; 14: 250-4.

14. **Zafiriou S, Stanners SR, Saad S, Polhill TS, Poronnik P, Pollock CA.** Pioglitazone inhibits cell growth and reduces matrix production in human kidney fibroblasts. *Journal of the American Society of Nephrology*. 2005; 16: 638-45.

15. **Jiang Y, Thakran S, Bheemreddy R, Ye E-A, He H, Walker RJ, Steinle JJ.** Pioglitazone normalizes insulin signaling in the diabetic rat retina through reduction in tumor necrosis factor α and suppressor of cytokine signaling 3. *Journal of Biological Chemistry*. 2014; 289: 26395-

405.

16. **Ko GJ, Kang YS, Han SY, Lee MH, Song HK, Han KH, Kim HK, Han JY, Cha DR.** Pioglitazone attenuates diabetic nephropathy through an anti-inflammatory mechanism in type 2 diabetic rats. *Nephrology Dialysis Transplantation*. 2008; 23: 2750-60.
17. **Jia H, Zhu S, Ji Q, Hui K, Duan M, Xu J, Li W.** Repeated administration of pioglitazone attenuates development of hyperalgesia in a rat model of neuropathic pain. *Experimental and clinical psychopharmacology*. 2010; 18: 359.
18. **Park S-W, Yi J-H, Miranpuri G, Satriotomo I, Bowen K, Resnick DK, Vemuganti R.** Thiazolidinedione class of peroxisome proliferator-activated receptor γ agonists prevents neuronal damage, motor dysfunction, myelin loss, neuropathic pain, and inflammation after spinal cord injury in adult rats. *Journal of Pharmacology and Experimental Therapeutics*. 2007; 320: 1002-12.
19. **Ahmadian M, Suh JM, Hah N, Liddle C, Atkins AR, Downes M, Evans RM.** PPARgamma signaling and metabolism: the good, the bad and the future. *Nature medicine*. 2013; 19: 557-66.
20. **Hur J, Dauch JR, Hinder LM, Hayes JM, Backus C, Pennathur S, Kretzler M, Brosius FC, 3rd, Feldman EL.** The Metabolic Syndrome and Microvascular Complications in a Murine Model of Type 2 Diabetes. *Diabetes*. 2015.
21. **Tamayo P, Slonim D, Mesirov J, Zhu Q, Kitareewan S, Dmitrovsky E, Lander ES, Golub TR.** Interpreting patterns of gene expression with self-organizing maps: methods and application to hematopoietic differentiation. *Proceedings of the National Academy of Sciences*. 1999; 96: 2907-12.
22. **Törönen P, Kolehmainen M, Wong G, Castrén E.** Analysis of gene expression data using self-organizing maps. *FEBS letters*. 1999; 451: 142-6.
23. **Nikkilä J, Törönen P, Kaski S, Venna J, Castrén E, Wong G.** Analysis and visualization of gene expression data using self-organizing maps. *Neural networks*. 2002; 15: 953-66.
24. **Sara A. Byron KRVK-J, David M. Engelthaler, John D. Carpten & David W. Craig.** Translating RNA sequencing into clinical diagnostics: opportunities and challenges. *Nature Reviews Genetics*. 2016.
25. **Rapaport F, Khanin R, Liang Y, Pirun M, Krek A, Zumbo P, Mason CE, Socci ND, Betel D.** Comprehensive evaluation of differential gene expression analysis methods for RNA-seq data. *Genome Biol*. 2013; 14: R95.
26. **Soneson C, Delorenzi M.** A comparison of methods for differential expression analysis of RNA-seq data. *BMC bioinformatics*. 2013; 14: 1.

27. **Biessels GJ, van der Heide LP, Kamal A, Bleys RL, Gispen WH.** Ageing and diabetes: implications for brain function. *Eur J Pharmacol*. 2002; 441: 1-14.
28. **Laboratory B.** Determination of Podocyte Number and Density in Rodent Glomeruli. Animal Models of Diabetic Complications Consortium.
29. **Sullivan KA, Hayes JM, Wiggin TD, Backus C, Su Oh S, Lentz SI, Brosius F, 3rd, Feldman EL.** Mouse models of diabetic neuropathy. *Neurobiol Dis*. 2007; 28: 276-85.
30. **Oh SS, Hayes JM, Sims-Robinson C, Sullivan KA, Feldman EL.** The effects of anesthesia on measures of nerve conduction velocity in male C57Bl6/J mice. *Neurosci Lett*. 2010; 483: 127-31.
31. **Zhang H, Saha J, Byun J, Schin M, Lorenz M, Kennedy RT, Kretzler M, Feldman EL, Pennathur S, Brosius FC, 3rd.** Rosiglitazone reduces renal and plasma markers of oxidative injury and reverses urinary metabolite abnormalities in the amelioration of diabetic nephropathy. *Am J Physiol Renal Physiol*. 2008; 295: F1071-81.
32. **Sanden SK, Wiggins JE, Goyal M, Riggs LK, Wiggins RC.** Evaluation of a thick and thin section method for estimation of podocyte number, glomerular volume, and glomerular volume per podocyte in rat kidney with Wilms' tumor-1 protein used as a podocyte nuclear marker. *Journal of the American Society of Nephrology : JASN*. 2003; 14: 2484-93.
33. **Zhang H, Saha J, Byun J, Schin M, Lorenz M, Kennedy RT, Kretzler M, Feldman EL, Pennathur S, Brosius FC.** Rosiglitazone reduces renal and plasma markers of oxidative injury and reverses urinary metabolite abnormalities in the amelioration of diabetic nephropathy. *American Journal of Physiology-Renal Physiology*. 2008; 295: F1071-F81.
34. **Sanden SK, Wiggins JE, Goyal M, Riggs LK, Wiggins RC.** Evaluation of a thick and thin section method for estimation of podocyte number, glomerular volume, and glomerular volume per podocyte in rat kidney with Wilms' tumor-1 protein used as a podocyte nuclear marker. *Journal of the American Society of Nephrology*. 2003; 14: 2484-93.
35. **Trapnell C, Roberts A, Goff L, Pertea G, Kim D, Kelley DR, Pimentel H, Salzberg SL, Rinn JL, Pachter L.** Differential gene and transcript expression analysis of RNA-seq experiments with TopHat and Cufflinks. *Nature protocols*. 2012; 7: 562-78.
36. **Bethunaickan R, Berthier CC, Zhang W, Eksi R, Li HD, Guan Y, Kretzler M, Davidson A.** Identification of Stage-Specific Genes Associated With Lupus Nephritis and Response to Remission Induction in (NZB× NZW) F1 and NZM2410 Mice. *Arthritis & Rheumatology*. 2014; 66: 2246-58.
37. **Demuth H, Beale M.** Neural network toolbox for use with MATLAB. 1993.

38. **Huang DW, Sherman BT, Lempicki RA.** Systematic and integrative analysis of large gene lists using DAVID bioinformatics resources. *Nature protocols*. 2008; 4: 44-57.
39. **O'Brien PD, Hur J, Hayes JM, Backus C, Sakowski SA, Feldman EL.** BTBR ob/ob mice as a novel diabetic neuropathy model: Neurological characterization and gene expression analyses. *Neurobiology of disease*. 2014; 73C: 348-55.
40. **Sas KM, Kayampilly P, Byun J, Nair V, Hinder LM, Hur J, Zhang H, Lin C, Qi NR, Michailidis G, Groop PH, Nelson RG, Darshi M, Sharma K, Schelling JR, Sedor JR, Pop-Busui R, Weinberg JM, Soleimanpour SA, Abcouwer SF, Gardner TW, Burant CF, Feldman EL, Kretzler M, Brosius FC, 3rd, Pennathur S.** Tissue-specific metabolic reprogramming drives nutrient flux in diabetic complications. *JCI Insight*. 2016; 1: e86976.
41. **Hinder LM, Vivekanandan-Giri A, McLean LL, Pennathur S, Feldman EL.** Decreased glycolytic and tricarboxylic acid cycle intermediates coincide with peripheral nervous system oxidative stress in a murine model of type 2 diabetes. *J Endocrinol*. 2013; 216: 1-11.
42. **Hinder LM, Figueroa-Romero C, Pacut C, Hong Y, Vivekanandan-Giri A, Pennathur S, Feldman EL.** Long-chain acyl coenzyme A synthetase 1 overexpression in primary cultured Schwann cells prevents long chain fatty acid-induced oxidative stress and mitochondrial dysfunction. *Antioxid Redox Signal*. 2014; 21: 588-600.
43. **Vincent AM, Calabek B, Roberts L, Feldman EL.** Biology of diabetic neuropathy. *Handbook of clinical neurology*. 2013; 115: 591-606.
44. **Russell JW, Sullivan KA, Windebank AJ, Herrmann DN, Feldman EL.** Neurons undergo apoptosis in animal and cell culture models of diabetes. *Neurobiol Dis*. 1999; 6: 347-63.
45. **Festing MF, Altman DG.** Guidelines for the design and statistical analysis of experiments using laboratory animals. *ILAR J*. 2002; 43: 244-58.
46. **Lappin DW, Hensey C, McMahon R, Godson C, Brady HR.** Gremlins, glomeruli and diabetic nephropathy. *Curr Opin Nephrol Hypertens*. 2000; 9: 469-72.
47. **Dolan V, Murphy M, Sadlier D, Lappin D, Doran P, Godson C, Martin F, O'Meara Y, Schmid H, Henger A, Kretzler M, Droguett A, Mezzano S, Brady HR.** Expression of gremlin, a bone morphogenetic protein antagonist, in human diabetic nephropathy. *Am J Kidney Dis*. 2005; 45: 1034-9.
48. **Kahvecioglu S, Guclu M, Ustundag Y, Gul CB, Dogan I, Dagel T, Esen B, Esen SA, Celik H, Esen I.** Evaluation of Serum Spondin 2 Levels in the Different Stages of Type 2 Diabetic Nephropathy. *Nephrology (Carlton)*. 2015.
49. **Salisbury EA, Lazard ZW, Ubogu EE, Davis AR, Olmsted-Davis EA.** Transient brown

adipocyte-like cells derive from peripheral nerve progenitors in response to bone morphogenetic protein 2. *Stem Cells Transl Med*. 2012; 1: 874-85.

50. **Niu H, Li Y, Li H, Chi Y, Zhuang M, Zhang T, Liu M, Nie L.** Matrix metalloproteinase 12 modulates high-fat-diet induced glomerular fibrogenesis and inflammation in a mouse model of obesity. *Scientific reports*. 2016; 6.

51. **Brownlee M.** The pathobiology of diabetic complications: a unifying mechanism. *Diabetes*. 2005; 54: 1615-25.

TABLES

Table 1. Pathway enrichment analysis of SOM Cluster. Top 20 significantly enriched canonical pathways among the shared genes in modules 42 and 49 from the SOM analysis using IPA*.

Canonical pathways	**BH P-value***	**Genes**
Mitochondrial Dysfunction	7.94E-20	*Ndufa4, Sdhb, Cox7b, Cox6a1, Cox6c, Prdx5, Uqcr11, Xdh, Aco2, Ndufb3, Ndufb10, Pdha1, Ndufb9, Ndufab1, Ndufb6, Aco1, Atp5g3, Cox4i1, Sdha, Ndufv1, Cox6b1, Ndufb4, Cycs, Ndufv3, Uqcrb, Gsr, Atp5b, Uqcr10, Uqcrc2, Cyc1, Cox5a, Cox7a2, Ndufa12, Atpaf2, Uqcrq*
Oxidative Phosphorylation	7.94E-20	*Ndufa4, Sdhb, Cox7b, Cox6a1, Cox6c, Uqcr11, Ndufb3, Ndufb10, Ndufb9, Ndufab1, Ndufb6, Atp5g3, Cox4i1, Sdha, Ndufv1, Cox6b1, Ndufb4, Cycs, Ndufv3, Uqcrb, Atp5b, Uqcr10, Uqcrc2, Cyc1, Cox5a, Cox7a2, Ndufa12, Atpaf2, Uqcrq*
TCA Cycle II (Eukaryotic)	3.16E-17	*Sdha, Sdhb, Idh3g, Aco2, Mdh1, Sucla2, Cs, Suclg1, Dlst, Dld, Idh3a, Mdh2, Fh, Aco1, Idh3b*
Glycolysis I	4.37E-07	*Pgk1, Eno1, Tpi1, Pgam1, Pkm, Aldoa, Gapdh, Pfkl, Aldoc*
Glutaryl-CoA Degradation	6.17E-06	*Hadhb, L3hypdh, Acat1, Ehhadh, Hsd17b4, Hadh*

Gluconeogenesis I	6.17E-06	*Pgk1, Eno1, Pgam1, Aldoa, Gapdh, Mdh1, Mdh2, Aldoc*
Valine Degradation I	7.41E-06	*Hadhb, Echs1, Bcat2, Bckdha, Dld, Dbt, Ehhadh*
Acetyl-CoA Biosynthesis I (Pyruvate Dehydrogenase Complex)	8.71E-06	*Pdha1, Dlat, Dld, Dbt, Pdhb*
Fatty Acid β-oxidation I	2.00E-05	*Hadhb, Echs1, Ehhadh, Hsd17b4, Acadm, Acaa2, Eci1, Hadh*
Isoleucine Degradation I	2.14E-05	*Hadhb, Echs1, Bcat2, Acat1, Dld, Ehhadh*
Tryptophan Degradation III (Eukaryotic)	2.19E-04	*Hadhb, L3hypdh, Acat1, Ehhadh, Hsd17b4, Hadh*
Sucrose Degradation V (Mammalian)	1.32E-03	*Tpi1, Aldoa, Galm, Aldoc*
Branched-chain α-keto acid Dehydrogenase Complex	1.70E-03	*Bckdha, Dld, Dbt*
Pentose Phosphate Pathway (Oxidative Branch)	3.89E-03	*Pgd, Pgls, G6pd*
Lipoate Biosynthesis and Incorporation II	1.55E-02	*Lipt1, Lias*
Leucine Degradation I	2.69E-02	*Bcat2, Acadm, Mccc2*
Ascorbate Recycling (Cytosolic)	3.55E-02	*Glrx, Gsto1*
Glutathione Redox Reactions II	3.55E-02	*Gsr, Glrx*
Fatty Acid β-oxidation III (Unsaturated, Odd Number)	3.55E-02	*Ehhadh, Eci1*
Pentose Phosphate Pathway	4.07E-02	*Pgd, Pgls, G6pd*

* IPA = Ingenuity Pathway Analysis, BH P-value: Benjamini-hochberg P-value

FIGURE LEGENDS

Figure 1. Study workflow. (A) *db/+* and *db/db* mice were treated with or without 15 mg/kg pioglitazone (112.5 mg pioglitazone/kg chow, for a final dose of 15 mg/kg to the mouse) from 5 wk-16 wk of age. (B) Total RNA from nerve and kidney tissues was isolated for RNA-Seq analysis. RNA-Seq

data were mapped, aligned, and used for differential expression and Self-Organizing Map analysis. The identified genes of interest were used for functional enrichment analysis. SCN, sciatic nerve; DRG, dorsal root ganglia; Glom, glomeruli; QA, quality assessment.

Figure 2. Differential expression analysis. RNA-Seq data were used to determine gene expression in nerve (SCN, DRG) and kidney (Glom, Cortex) tissues from all groups. (A) Differential gene expression analysis was determined using Cuffdiff with a false discovery rate (FDR) cutoff of < 0.05. Pairwise comparisons were performed between DEG sets for all groups within a tissue. DEGs regulated by both diabetes and pioglitazone within a tissue were determined (*db/+* vs. *db/db* and *db/db* vs. *db/db* PIO). Venn diagrams illustrate the shared and unique DEGs between the two groups. (B) Directionality of regulation of these overlapping DEG sets was assessed, and the shared genes were divided into two groups: DEGs Reversed by PIO and DEGs Exacerbated by PIO. (C) The percentage of shared DEGs exacerbated and reversed by PIO is indicated in the pie chart for each tissue. SCN, sciatic nerve; DRG, dorsal root ganglia; Glom, glomeruli.

Figure 3. Analysis of DEGs between SCN and glomeruli. The DEG sets were analyzed between the DEGs reversed by pioglitazone treatment in glomeruli and three groups of DEGs in SCN: (A) SCN *db/db* only, (B) SCN Exacerbated, and (C) SCN Reversed. (D) DAVID functional enrichment analysis was performed on the shared DEGs from each comparison. Over-represented functions are shown in the heat map with P-value < 0.05.

Figure 4. Analysis of Self-Organizing Maps. SOM analysis was applied to the RNA-Seq data to identify coherent patterns of gene expression across six groups: *db/+*, *db/db*, and *db/db* PIO in SCN and glomeruli. (A) SOM clustering analysis demonstrates the distances between correlated gene groups. Small blue hexagons represent a module containing genes with a similar expression pattern. The neighboring modules are connected with a red line. The colors between the modules indicate the similarity between modules: lighter colors represent higher similarity and darker colors represent lower similarity. (B) Gene expression patterns of biological interest were identified, and a Cluster comprised of modules 42 and 49 was further analyzed.

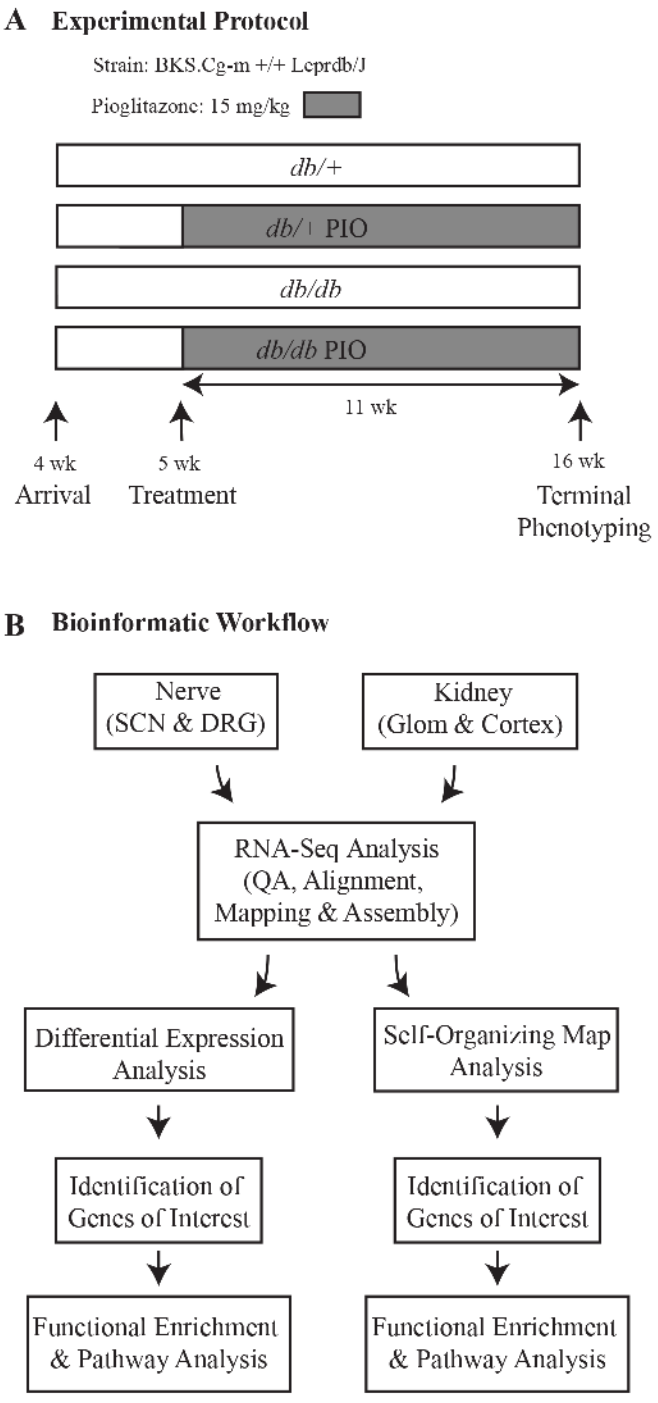

jcmm_13136_f1.tif

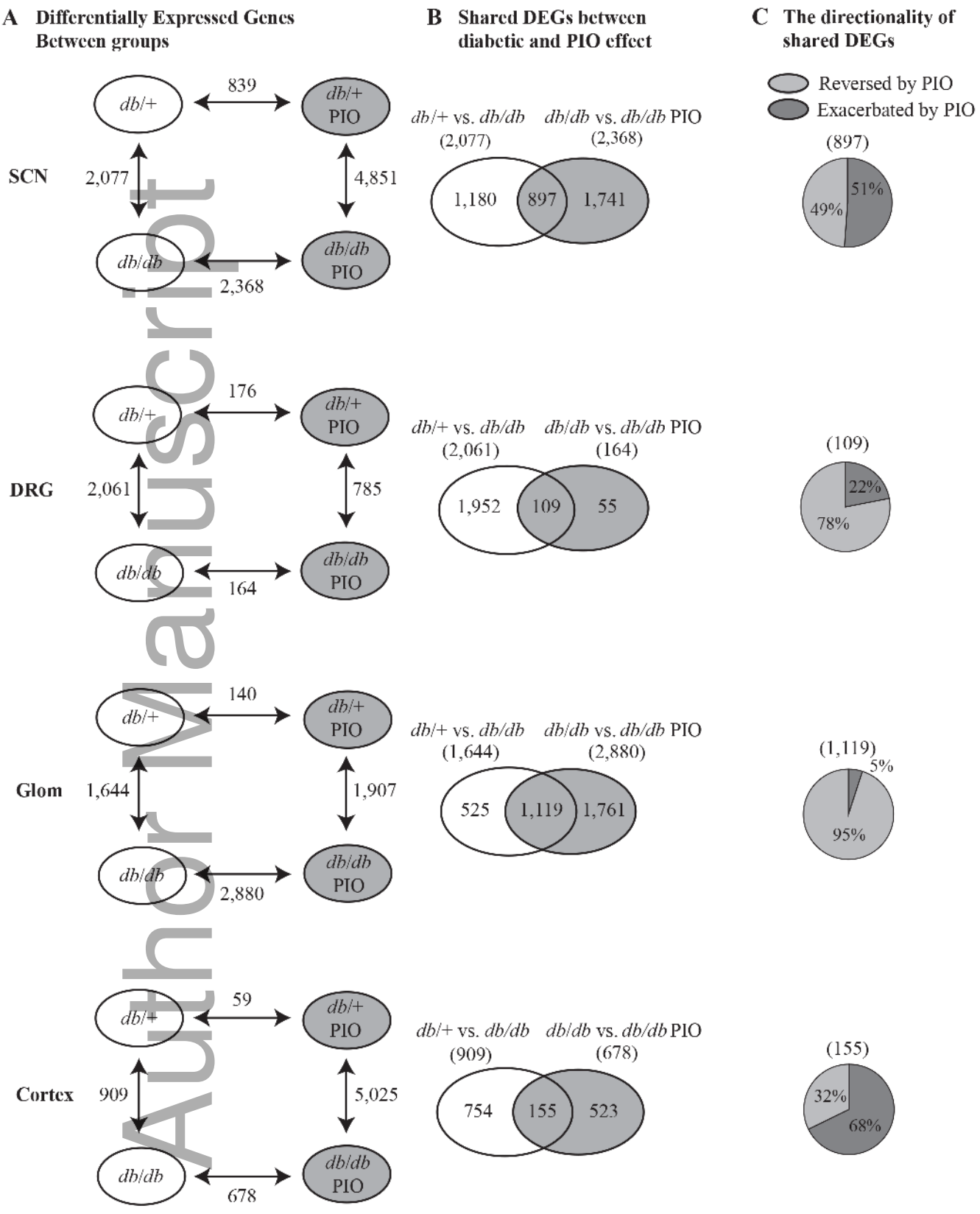

jcmm_13136_f2.tif

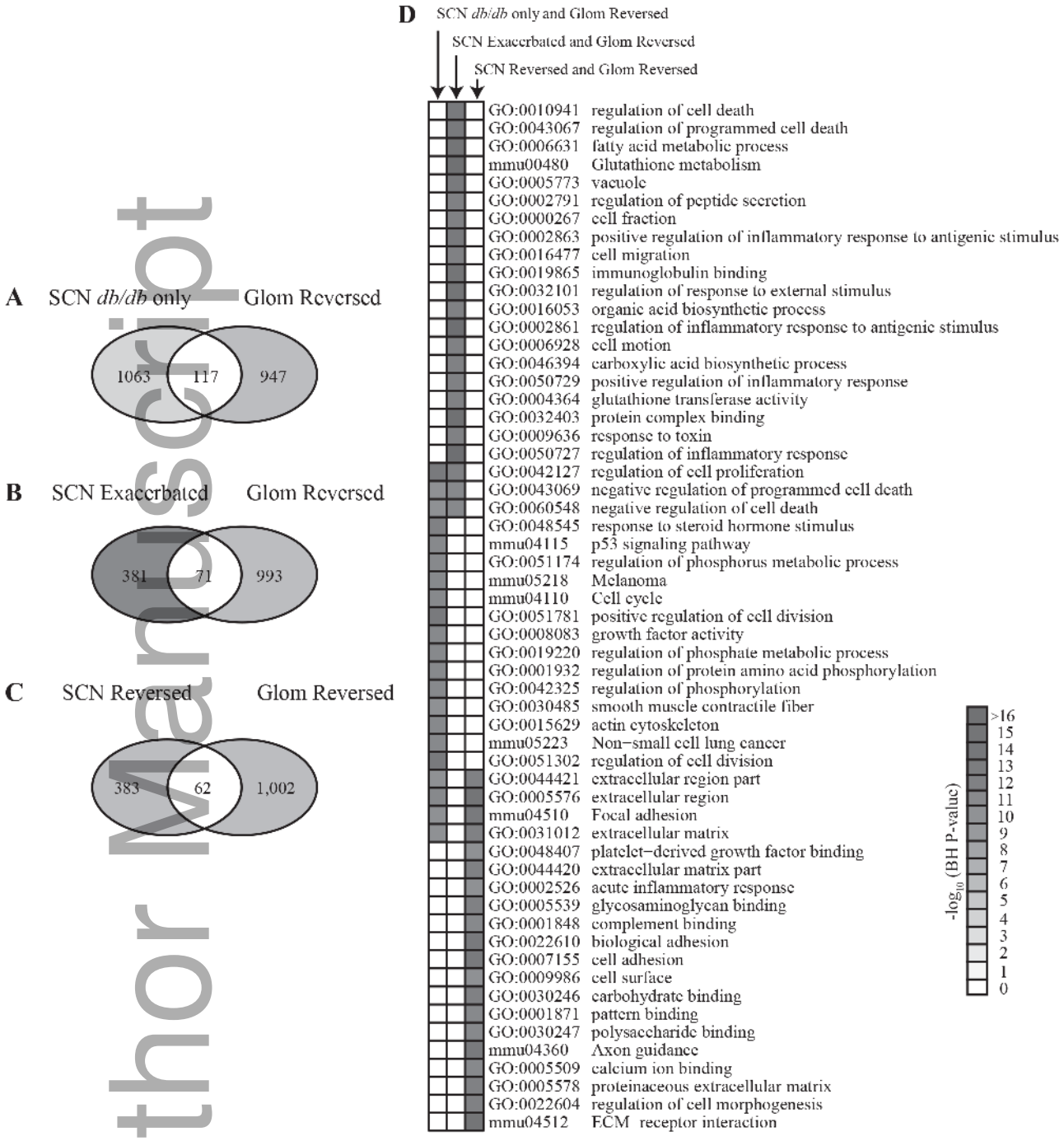

jcmm_13136_f3.tif

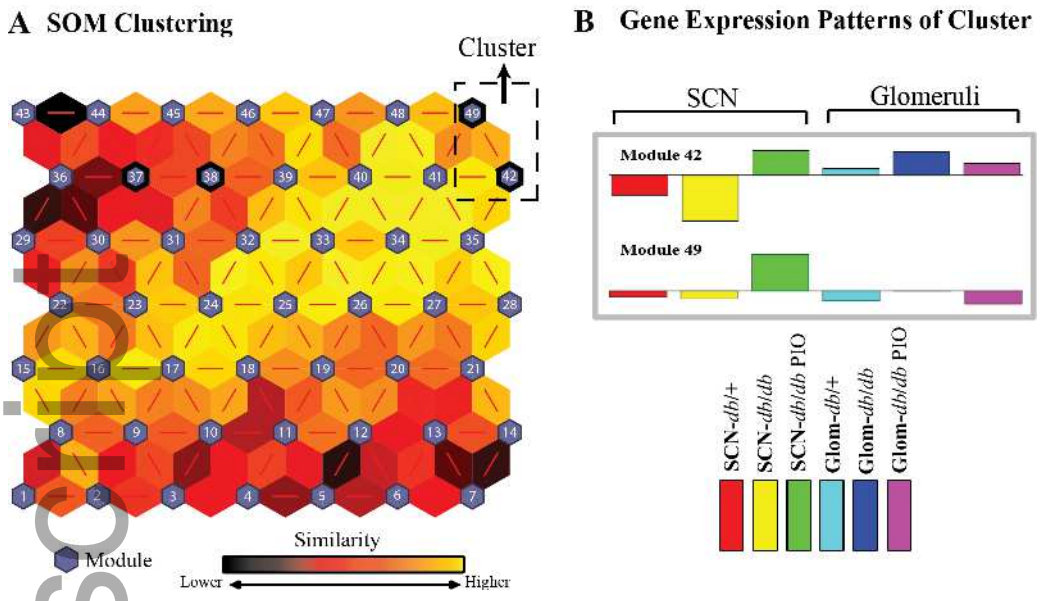

jcmm_13136_f4.tif